Remote Sensing of Environment 206 (2018) 33–44

Contents lists available at ScienceDirect

Remote Sensing of Environment

journal homepage: www.elsevier.com/locate/rse

Improved crop residue cover estimates obtained by coupling spectral indices for residue and moisture

M. Quemada[a,*], W.D. Hively[b], C.S.T. Daughtry[c], B.T. Lamb[d], J. Shermeyer[b]

[a] School of Agricultural Engineering, CEIGRAM, Universidad Politécnica de Madrid, Madrid 28040, Spain
[b] U.S. Geological Survey, Eastern Geographic Science Center, Reston, VA 20190, USA
[c] U.S. Department of Agriculture, Agricultural Research Service, Hydrology and Remote Sensing Laboratory, Beltsville, MD 20705, USA
[d] Department of Earth and Atmospheric Sciences, City College of New York, City University of New York, NY 10031, USA

ARTICLE INFO

Keywords:
Conservation agriculture
Non-photosynthetic vegetation
Normalized difference tillage index
Shortwave infrared normalized difference residue index
Tillage intensity
Water content index
Worldview-3

ABSTRACT

Remote sensing assessment of crop residue cover (f_R) and tillage intensity can improve predictions of the environmental impact of agricultural practices and promote sustainable management. Spectral indices for estimating f_R are sensitive to soil and crop residue water contents, therefore the uncertainty of f_R estimates increases when moisture conditions vary. Our goals were to evaluate the robustness of spectral residue indices based on the shortwave infrared region (SWIR) for estimating f_R and to mitigate the uncertainty caused by variable moisture conditions on f_R estimates. Ten fields with center pivot irrigation systems (eight partially irrigated and two uniformly dry fields) were identified in Worldview-3 satellite imagery acquired for a study site in Maryland (USA). The fields were mid-irrigation at the time of imagery acquisition, allowing comparison of residue cover under dry and wet conditions. Fields were subdivided into approximately equal-size wedges within the dry and wet portions of each field, and the SWIR bands were extracted for each pixel. Two crop residue indices (Normalized Difference Tillage Index (NDTI); Shortwave Infrared Normalized Difference Residue Index (SINDRI) and a water index (WI) were calculated. Reflectance in each band was moisture-adjusted based on the WI difference between wet and dry wedges, and updated NDTI and SINDRI were calculated. Finally, the probability density distributions of f_R estimated from the residue indices were calculated for each field. SINDRI was more robust than NDTI for estimating f_R. Moisture corrections of spectral bands reduced the root mean square error of NDTI f_R estimates from 22.7% to 4.7%, and SINDRI f_R estimates from 6.0% to 2.2%. The mean and variance of the probability density distribution of f_R estimated from residue indices, before and after moisture correction, were greatly reduced in the partially irrigated fields, but only slightly in fields with uniform water distribution. The estimation of f_R should be based on SINDRI if appropriate bands are available, but f_R can be reliably estimated by combining NDTI with a water content index to mitigate the uncertainty caused by variable moisture conditions.

1. Introduction

Maintaining crop residues on the soil surface is a key component of conservation agriculture promoted by the Food and Agriculture Organization of the United Nations to make more sustainable cropping systems (FAO, 2015). The soil is often completely covered by crop residues after harvest, but residue cover decreases as the soil is tilled or residues are removed for fuel or feed. Crop residue fractional cover (f_R) reduces soil erosion and runoff, and therefore the amount of nutrients and agrochemicals that reach surface waters (Delgado, 2010). Tillage intensity is the main management practice that controls f_R and a reduction in tillage is associated with increasing soil organic matter and water retention capacity (Hobbs et al., 2008). In addition, tillage intensity is often a key variable in models, such as EPIC (Izaurralde et al., 2006) and SWAT (Gassman et al., 2007), that predict the overall impact of agricultural systems on soil organic carbon, greenhouse gas emissions, and water quality. These models require geospatial information on landscape topography, soil properties, weather and climate, crop type and management practices, including soil tillage intensity. Appropriate databases exist for all of these requirements except for soil tillage intensity. Thus, the capability to assess f_R and soil tillage intensity can help to improve predictions of the impact of agricultural practices across landscapes and further promote sustainable management of our resources.

* Corresponding author.
E-mail address: miguel.quemada@upm.es (M. Quemada).

https://doi.org/10.1016/j.rse.2017.12.012
Received 12 May 2017; Received in revised form 28 November 2017; Accepted 8 December 2017

Table 1
Spectral bands used for the crop residue cover indices SINDRI (Shortwave Infrared Normalized Difference Residue Index) and NDTI (Normalized Difference Tillage Index) and the water index (WI).

Band[a]	Wavelengths, nm		Equation	Reference
Residue index				
SWIR6	2185–2225	SINDRI	$\frac{100\,(SWIR6 - SWIR7)}{SWIR6 + SWIR7}$	Serbin et al., 2009
SWIR7	2235–2285			
OLI6	1570–1650	NDTI	$\frac{OLI6 - OLI7}{OLI6 + OLI7}$	Van Deventer et al., 1997
OLI7	2110–2290			
Water index				
SWIR3	1640–1680	WI	$\frac{SWIR3}{SWIR5}$	Quemada and Daughtry (2016)
SWIR5	2145–2185			

[a] SWIR3, SWIR5, SWIR6 and SWIR7 are Worldview-3 bands at the designated wavelengths; and OLI6 and OLI7 are Landsat OLI bands simulated with Worldview-3 [OLI6 = average bands (2, 3, 4), OLI7 = average bands (5, 6)].

Currently, in selected counties in the U.S., only qualitative information on crop residue management is available from farmer interviews and road-side surveys (CTIC, 2015). The quantitative standard used by the U.S. Department of Agriculture-Natural Resources Conservation Service (USDA-NRCS), the line-point transect, is impractical for wide-scale use because of time and human resources constraints (Corak et al., 1993; Thoma et al., 2004). Only remote sensing has the potential for monitoring f_R over large areas in a timely and cost effective manner (Zheng et al., 2014).

Early remote sensing methods for assessing f_R were often based on the relatively broad spectral bands of Landsat and similar satellites (Biard and Baret, 1997). Although these multispectral satellites typically have only a few relatively broad spectral bands, they provide global coverage and have been used to assess f_R at regional scales (Van Deventer et al., 1997; Thoma et al., 2004; Sullivan et al., 2008; Zheng et al., 2012). The Normalized Difference Tillage Index (NDTI) (Van Deventer et al., 1997) is generally one of the best of the Landsat-based tillage indices for estimating f_R (Table 1). The corresponding bands of Landsat 4 and 5 Thematic Mapper (TM), Landsat 7 Enhanced Thematic Mapper (ETM +), Landsat 8 Operational Land Imager (OLI), and Sentinel-2 may be used.

For the Landsat bands, the differences in reflectance of soils and crop residues are small and the accuracy of estimating f_R is often poor (Serbin et al., 2009; Quemada and Daughtry, 2016). However, in the 2100–2350 nm wavelength region, crop residues have absorption features associated with cellulose and lignin that are absent in the spectra of soils and green vegetation (Kokaly and Clark, 1999). Various spectral indices based on detecting these absorption features have been proposed (Daughtry, 2001; Serbin et al., 2009), but are not available using Landsat.

Advanced multispectral imagers, e.g., the Worldview-3 (WV-3) (SIC, 2017) and Advanced Spaceborne Thermal Emission and Reflection radiometer (ASTER) (Abrams, 2000), include multiple bands in the cellulose and lignin absorption region. The most robust crop residue index for these advanced multispectral sensors is the Shortwave Infrared Normalized Difference Residue Index (SINDRI) (Serbin et al., 2009), which can be calculated using the SWIR band 6 (2185–2225 nm) and 7 (2235–2285 nm) of WV-3 (Table 1). These WV-3 bands also correspond to ASTER bands A6 and A7. However, the ASTER SWIR sensor is no longer available due to detector failure in April 2008. Worldview-3 has 3.7-m spatial resolution for the SWIR bands, and is well suited for studying episodic events, but its narrow swath width is not suited for mapping large areas in a timely manner.

Water in the crop residues and soils reduces reflectance at all wavelengths, attenuates the cellulose and lignin absorption features, and reduces the contrast between soil and crop residues (Daughtry and Hunt, 2008; Wang et al., 2013). Thus, the uncertainty of f_R estimates increases as moisture content of the soil and residue increases, and any method to accurately monitor soil tillage intensity must account for variations in water content. Quemada and Daughtry (2016) showed that SINDRI and NDTI accurately estimated f_R when moisture conditions were relatively dry (i.e., relative water content (RWC) < 0.25), but when scene moisture conditions varied from dry to wet the uncertainty of f_R estimates increased. Although SINDRI was more robust to changes in moisture conditions than NDTI, a multivariate linear model that used pairs of spectral indices, one for RWC and one for f_R, improved estimates of f_R using SINDRI. In contrast, NDTI was very sensitive to water content and corrections were unreliable when RWC > 0.25.

In practice, water contents of soils and crop residues often vary spatially due to minor changes in local topographic relief. Therefore, a robust protocol is required to estimate f_R from indices calculated using satellite imagery under varying moisture conditions.

Our goal is to propose a method that mitigates the uncertainty caused by variable moisture conditions on remotely sensed estimates of crop residue cover. Specific objectives were to 1) evaluate the robustness of SWIR-based spectral residue indices under various moisture conditions and 2) develop a reliable method to mitigate the uncertainty caused by variable moisture conditions on estimates of crop residue cover. To achieve this goal, we compared the dry and wet portions of partially-irrigated fields that had been captured mid-irrigation by WV-3 imagery, assuming that residue cover was consistent across each field.

2. Material and methods

2.1. Dataset of field satellite images

Space-borne WV-3 images were acquired on 14 May 2015 over a study site in the Choptank River watershed of eastern Maryland (USA) (Fig. 1). These images were inspected and determined to be properly projected and free of clouds over the study site fields, thus no re-projection or cloud masking were performed. MODTRAN (Spectral Sciences Inc., Burlington, MA, US) was used for atmospheric correction, producing coefficients for converting image radiance values to surface reflectance values. R software was used to apply MODTRAN coefficients to radiance imagery and to output surface reflectance imagery. Individual surface reflectance images were then mosaiced to cover the region of study using ENVI (Harris Geospatial, Boulder, CO, USA).

On the day of imagery acquisition soils were somewhat dry, and irrigation was underway on a number of fields. The dataset used in this paper was composed of 10 fields with full or semi-circular irrigation pivots identified in the WV-3 images. When the images were acquired (12:06 Eastern Daylight Time), the irrigation systems in fields 1 to 8 were operating and, as a result, these fields had clearly identifiable areas with differing water content due to irrigation status (recently irrigated versus not-yet-irrigated). Inside each field, various wet and dry wedges were differentiated based on visual analysis of the image. For each of the wedges, the SWIR bands were extracted from each pixel and the mean and standard error were calculated (Table 2). The 3.7 m resolution of WV-3 image was resample to 4 m. The average size of each wedge was 9433 m^2, each pixel represented 16 m^2 and, therefore, the average number of pixels per wedge was 590. The wedge in which each pivot arm was actively spraying water was deleted, along with various anomalies such as wheel tracks and shallow drainage ditches.

Fields 9 and 10 had not been recently irrigated and thus had relatively uniform water contents when the WV-3 image was acquired. They were chosen to provide a measure of uniformity of the indices in the absence of irrigation. Both fields were subdivided into wedges following the procedure defined for fields 1–8 providing a measure of the expected spatial variation of WI and f_R within a field. The complete dataset contained 10 fields and 98 wedges. Fig. 1c shows an example of identified fields.

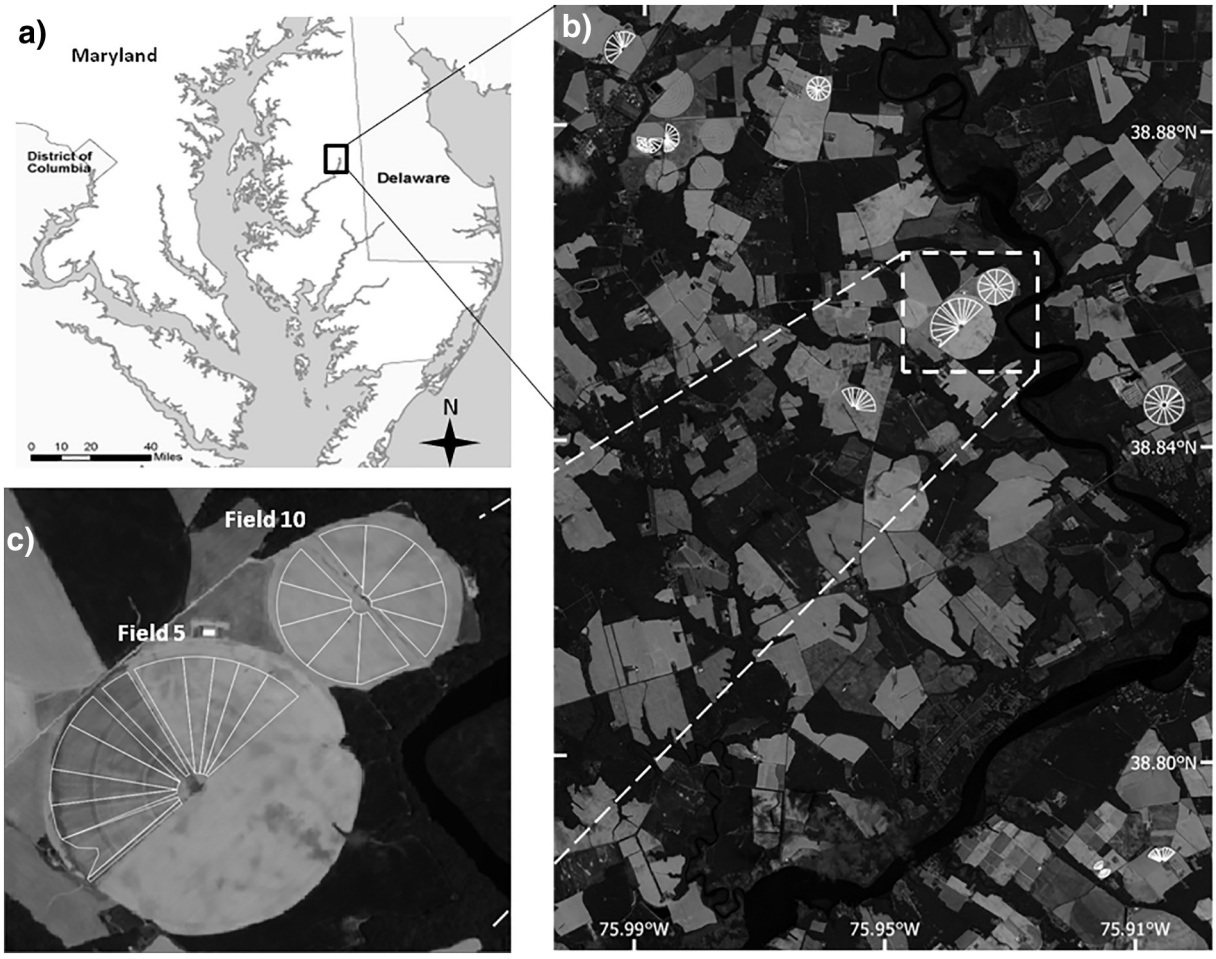

Fig. 1. Location of fields in the Worldview-3 image from Tuckahoe watershed in eastern Maryland (USA) acquired on 14 May 2015 (a, b), and detailed of a partially irrigated field with different water content areas (field 5) and with uniform water content distribution (Field 10).

Table 2
Field ID and location, area, number of pixels, type of crop residue, and number (n) of wet and dry wedges within each particular field. The mean values of water index (WI), Relative water content (RWC), Normalized Difference Tillage Index (NDTI), Shortwave Infrared Normalized Difference Residue Index (SINDRI) before and after moisture correction (NDTI*, SINDRI*) for the wedges of each field is provided. Fields without distinction between wedges wetness had uniform moisture conditions and were subdivided into East and West.

Field ID	Area (ha)	Pixels number	Type of crop residue	Wedges within each particular field							
				Type	n	WI	RWC[a]	Before moisture correction		After moisture correction	
								NDTI	SINDRI	NDTI*	SINDRI*
1	7.74	4839	Maize	Dry	3	1.144‡	0.34‡	0.102‡	3.30‡	0.105‡	3.29
				Wet	4	1.342‡	0.76‡	0.173‡	4.22‡	0.094‡	3.40
2	3.58	2236	Maize, barley	Dry	5	1.082‡	0.21‡	0.075‡	2.07‡	0.074	2.05
				Wet	4	1.362‡	0.80‡	0.181‡	3.48‡	0.077	2.09
3	4.74	2965	Maize, barley, wheat	Dry	4	1.100‡	0.24‡	0.083‡	2.09‡	0.081	2.07
				Wet	6	1.361‡	0.80‡	0.181‡	3.39‡	0.081	2.14
4	6.81	4257	Soybean, wheat	Dry	3	1.269‡	0.61‡	0.150‡	6.19‡	0.148	6.17
				Wet	3	1.322‡	0.72‡	0.168‡	6.42‡	0.145	6.16
5	21.50	13,435	Maize, soybean	Dry	5	1.004‡	0.04‡	0.045‡	0.59‡	0.044‡	0.58
				Wet	6	1.072‡	0.19‡	0.067‡	0.84‡	0.055‡	0.62
6	20.92	13,075	Maize	Dry	8	1.185‡	0.43‡	0.116‡	2.05‡	0.109	2.02
				Wet	6	1.247‡	0.56‡	0.133‡	2.21‡	0.104	1.99
7	3.12	1953	Maize	Dry	4	1.267‡	0.60‡	0.139‡	4.62‡	0.142	4.63
				Wet	3	1.396‡	0.88‡	0.183‡	5.07‡	0.131	4.32
8	1.96	1226	Maize	Dry	6	1.047‡	0.13‡	0.054‡	1.84‡	0.052‡	1.83
				Wet	5	1.166‡	0.39‡	0.104‡	2.16‡	0.073‡	1.83
9	7.17	4479	Maize	East	7	1.037	0.11	0.055	1.44	0.053	1.33
				West	6	1.039	0.12	0.056	1.49	0.054	1.35
10	14.90	9315	Maize, barley	East	5	1.048	0.13	0.059	1.32	0.058	1.34
				West	5	1.040	0.12	0.056	1.32	0.055	1.34

[a] RWC estimated from Quemada and Daughtry (2016): RWC = 2.0 * WI − 2.1.
‡ Within a field, significant difference between wet and dry wedge type according to Fisher's LSD at a 0.05 probability level.

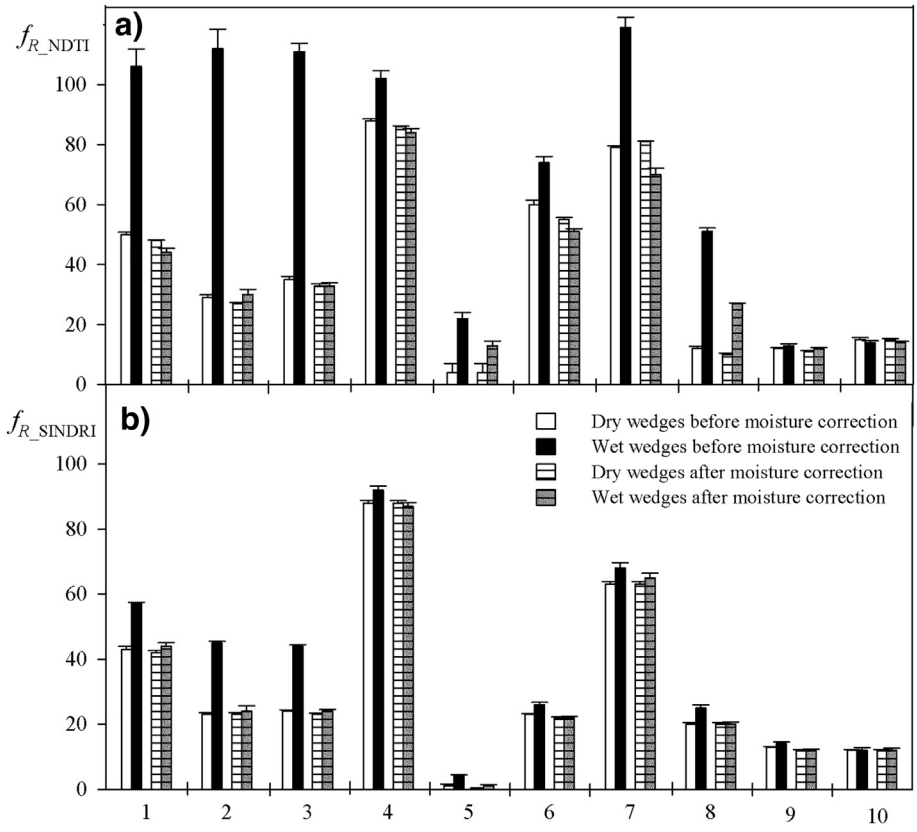

Fig. 2. Crop residue cover estimated from A) the Normalized Difference Tillage Index (f_{R_NDTI}) and B) the Shortwave Infrared Normalized Difference Residue Index (f_{R_SINDRI}) in the dry and the wet wedges of the various fields before and after moisture correction. Fields 9 and 10, as moisture distribution was uniform, were subdivided in East and West wedges for comparison purposes.

2.2. Dataset of f_R field measurements

Crop residue cover was measured in two fields, one almost completely covered by residues (field 4) and another almost completely bare soil (field 5). We used a digital camera (Canon G15) mounted on a pole at 2.14 m above the soil at a 0° view zenith angle and acquired 10 images per field (spatial resolution < 1 mm) at 3–5 m intervals along two transects in each field. The fractions of green vegetation, crop residue, and soil in each image were determined visually using SamplePoint software (Booth et al., 2006). The numbers of crosshairs that intersected green vegetation, crop residue or soil were counted, and f_R was calculated as the proportion of crop residue points in each image. The total number of crosshairs per image was 132. We divided the images among four analysts. When each analyst evaluated the same subset of 10 images, the root mean square error was < 4%. Green vegetation was < 3% in all images. The residues in the fields were from maize (*Zea mays* L.), soybean (*Glycine* max Merr.), barley (*Hordeum vulgare* L.) and wheat (*Triticum aestivum* L.) crops (Table 2).

2.3. Crop residue and water content indices

Spectral indices defined in Table 1 were calculated for each pixel in each of the wedges (Table 2). In addition, the relative water content (RWC) for each pixel was estimated using the spectral water index previously proposed in the literature to estimate crop residue and soil moisture conditions (Quemada and Daughtry, 2016). Reflectance factors for Landsat OLI bands (NASA, 2017; SIC, 2017) were estimated using WV-3 bands.

Crop residue cover measured through photographic analysis in dry wedges of fields 4 and 5 was linearly related to NDTI [Eq. (1)] and SINDRI [Eq. (2)]:

$$f_{R\_NDTI} = 789.07 * \text{NDTI} - 30.774 \quad (1)$$

$$f_{R\_SINDRI} = 15.69 * \text{SINDRI} - 9.194 \quad (2)$$

where, f_{R_NDTI} and f_{R_SINDRI} are crop residue covers estimated using NDTI and SINDRI, respectively. Both equations were highly significant ($p < 0.001$, adjusted $r^2 > 0.99$).

2.4. Analysis of variability

We calculated the mean and standard error of NDTI, SINDRI, and WI for each of the wedges in each field. The calibration equations were then used to estimate f_R for each wedge using either NDTI or SINDRI. We assumed that each field had uniform f_R among wedges, and that f_R differences within a field were due to inherent spatial variability in residue cover. To evaluate the moisture effect, the driest wedge (i.e. the one with a lower WI) in each field was selected and its f_R calculated using Eqs. (1) and (2). We also assumed f_R for each driest wedge was representative for the entire field. The variability within a field was evaluated as the root mean square error (*RMSE*) of the f_R estimated for all the wedges with respect to the driest, following the equation:

$$RMSE = \frac{1}{n}\sqrt{\sum_{i}^{n} (f_{R\,i} - f_{R\ driest\ wedge})^2} \quad (3)$$

where, n is the number of wedges in each field, $f_{R\,i}$ is the residue cover in wedge i, and $f_{R\ driest\ wedge}$ is the residue cover in the driest wedge of a particular field. Finally, the total error of fields with non-uniform water distribution ($RMSE_{Non}$) was calculated as the mean of the *RMSE* of individual fields from 1 to 8. The percent reduction of the *RMSE* (*% RMSE*) was calculated as the difference between the *RMSE* before and after moisture correction with respect to the *RMSE* before the correction.

The variability of f_R within each field was also evaluated by calculating the *Range* as the difference between the maximum and the minimum mean f_R of the wedges within each field. The maximum variability of the dataset ($Range_{max}$) was obtained as the largest range of the whole dataset.

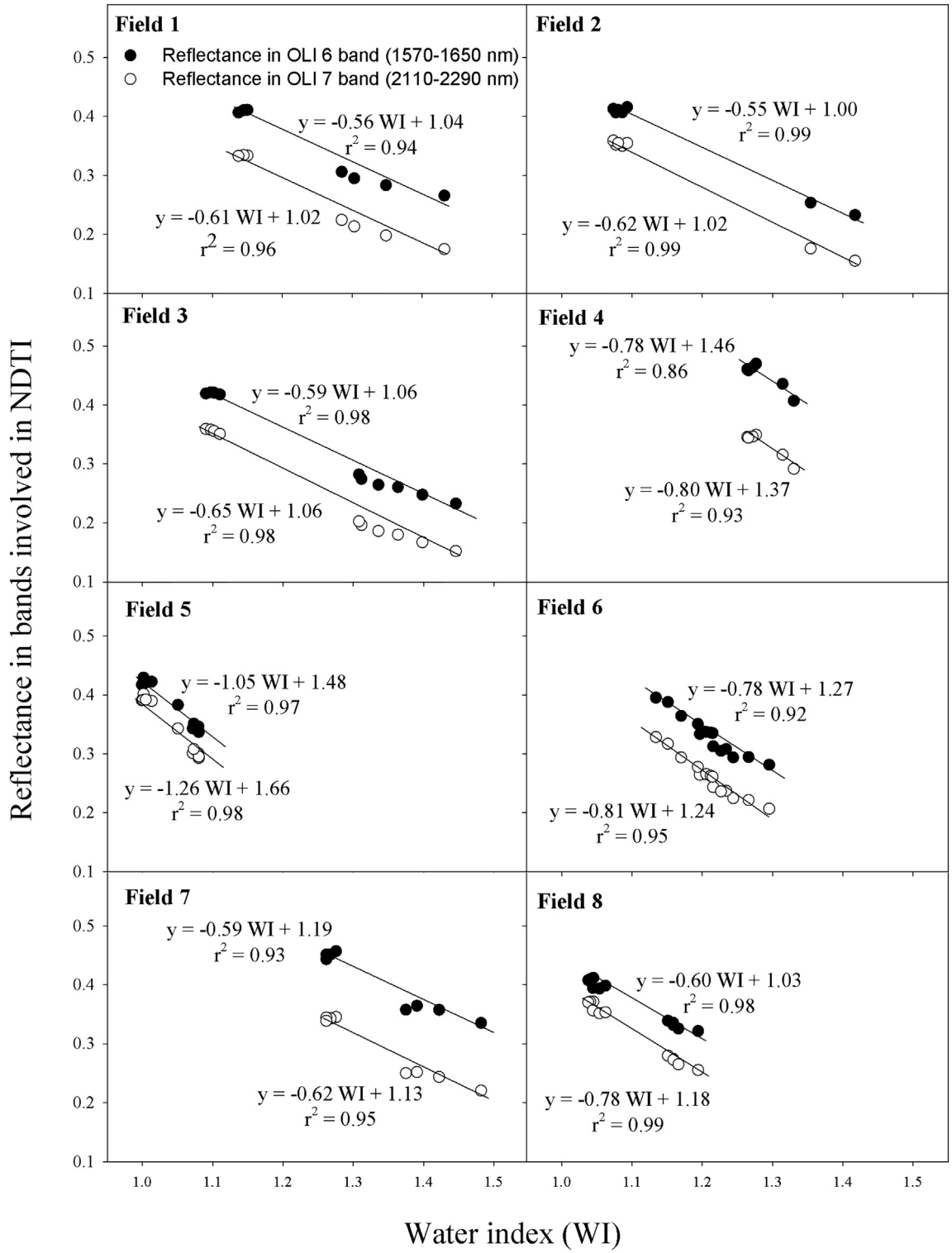

Fig. 3. Changes in reflectance bands OLI 6 (1570–1650 nm) and 7 (2110–2290 nm) of Landsat OLI satellite as function of the water index.

2.5. Moisture correction

Water content of soils and crop residues affected the reflectance factors of all SWIR bands used to calculate f_R. The reflectance factor of each band was plotted against the WI as an indicator of relative water content (RWC) of the crop residues and soils. Reflectance in each band was moisture-adjusted for each wedge ($Ref^*_{band\ i}$) by adding to the measured reflectance in the wedge ($Ref_{band\ i}$) the product of the difference in WI between the actual wedge (WI_i) and the driest wedge in the field ($WI_{driest\ wedge}$) multiplied by the slope of the linear relationship between the SWIR bands involved in the residue index calculation ($slope_{band}$) and the WI, following the equation:

$$Ref^*_{band\ i} = Ref_{band\ i} + slope_{band} \cdot (WI_i - WI_{driest\ wedge}) \quad (4)$$

The *slope* was optimized to obtain the minimum $RMSE_{Non}$. Moisture-adjusted reflectance values were used to calculate moisture-adjusted NDTI and SINDRI (called NDTI* and SINDRI*) which, in turn, were used for moisture-adjusted f_R for each index using either Eqs. (1) or (2).

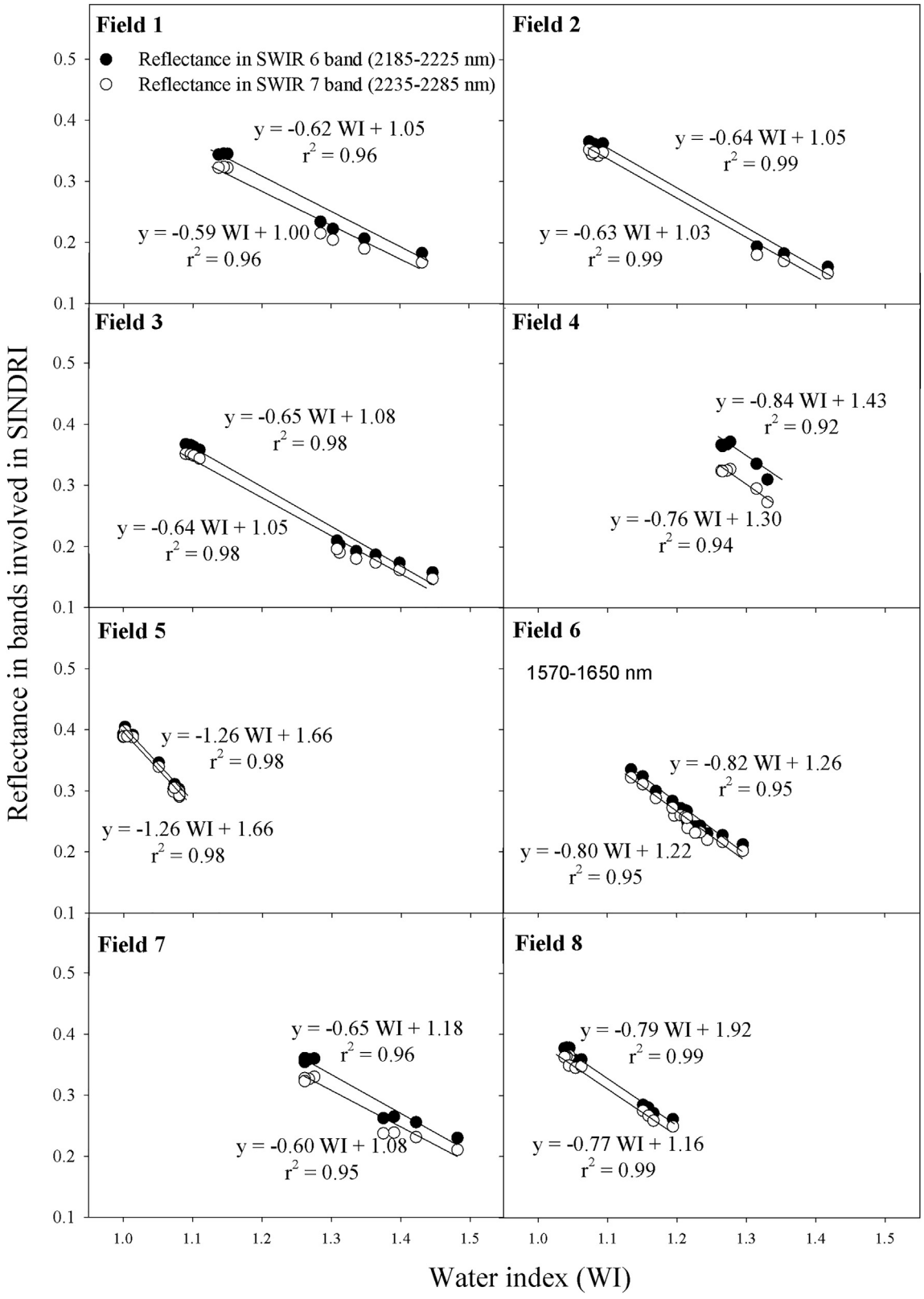

Fig. 4. Changes in reflectance bands SWIR 6 (2185–2225 nm) and 7 (2235–2285 nm) of Worldview-3 satellite as function of water index.

Table 3
Variation (*RMSE* and *Range*) for residue cover estimated using NDTI and SINDRI before (f_{R_NDTI}, f_{R_SINDRI}) and after ($f_{R\_NDTI_*}$, $f_{R\_SINDRI_*}$) moisture correction for each field, and for all the fields with non-uniform water distribution ($RMSE_{Non}$ and $Range_{max}$). The *% RMSE* shows the percent reduction of the *RMSE* before and after the moisture correction with respect to the *RMSE* before the correction.

Field ID	Before moisture correction				After moisture correction					
	f_{R_NDTI}		f_{R_SINDRI}		$f_{R\_NDTI_*}$			$f_{R\_SINDRI_*}$		
	RMSE	*Range*	*RMSE*	*Range*	*RMSE*	*% RMSE*	*Range*	*RMSE*	*% RMSE*	*Range*
Fields with non-uniform water distribution										
1	33.8	81	9.9	17	2.7	92†	11	2.8	72†	12
2	30.6	100	9.8	25	2.3	93†	7	2.7	72†	8
3	50.0	102	12.0	24	3.2	94†	11	2.0	83†	8
4	6.3	18	2.5	7	1.0	84†	4	1.7	32†	7
5	13.3	31	2.4	8	9.2	31†	20	2.0	17	8
6	14.2	47	2.5	10	4.8	66†	21	1.1	57†	6
7	11.9	42	5.5	14	2.9	84†	12	2.8	51†	11
8	21.7	52	3.4	12	10.1	54†	20	2.5	27†	9
$RMSE_{Non}$	23.4		6.0		4.5	81†		2.2	63†	
$Range_{max}$		102		25			21			12
Fields with uniform water distribution										
9	4.9	8	1.7	5	3.8	22	6	1.5	9	5
10	5.1	9	3.9	7	3.6	28	7	3.8	1	7

† The reduction of the *RMSE* before and after the moisture correction was significant at $p < 0.05$.

Table 4
Mean and variance of the density probability distribution of all pixels in each field for the water index and for residue cover estimated using NDTI and SINDRI before (f_{R_NDTI}, f_{R_SINDRI}) and after ($f_{R\_NDTI_*}$, $f_{R\_SINDRI_*}$) moisture correction.

Field ID	Water index		Before moisture correction				After moisture correction			
			f_{R_NDTI}		f_{R_SINDRI}		$f_{R\_NDTI_*}$		$f_{R\_SINDRI_*}$	
	Mean	Variance	Mean	Variance	Mean	Variance	Mean	Variance	Mean	Variance
1	1.28	0.012	88	897.6	52	85.6	45	19.6	40	46.8
2	1.22	0.021	70	1839.5	35	225.7	28	17.7	24	61.7
3	1.28	0.016	89	1319.9	38	271.4	33	23.1	25	112.7
4	1.29	0.002	92	118.1	89	80.0	85	9.0	87	63.9
5	1.04	0.002	15	241.0	2	77.6	9	77.1	2	65.9
6	1.21	0.003	66	267.6	24	85.6	52	14.7	22	68.5
7	1.32	0.007	93	440.2	65	60.9	77	55.5	63	54.1
8	1.10	0.004	29	456.0	22	143.5	18	75.6	20	106.9
9	1.04	0.0001	12	23.9	13	32.7	11	13.1	13	31.7
10	1.04	0.0001	15	21.9	11	24.8	14	11.0	11	24.6

To evaluate the performance of the moisture correction, the $RMSE_{Non}$ and the $Range_{max}$ were calculated for the moisture-corrected dataset.

Finally, the moisture correction was applied to all the individual pixels in the 10 fields, and moisture-corrected average index values per wedge were calculated. The probability density distributions of WI and f_R estimated from the residue indices, before and after the moisture correction, were calculated for each field.

3. Results

3.1. Indices and f_R estimation

In the fields that were partially irrigated, the WI, NDTI, and SINDRI were significantly higher in the wet wedges than in the dry wedges (Table 2). As a consequence, the mean f_R of the wet wedges was overestimated in fields 1 to 8 compared to the dry wedges (Fig. 2). For five of the fields, mean f_R estimated using NDTI was > 100% for the wet wedges. For all partially irrigated fields, the ratio between the mean f_R estimated from NDTI in the wet and dry wedges was > 2, whereas between the mean f_R estimated from SINDRI was ≈ 1.3.

In the non-irrigated fields without distinction between wedges wetness (fields 9 and 10), no significant differences were observed between the wedges in either NDTI or SINDRI, as a result the mean f_R was established to be uniform (Table 2; Fig. 2). The lack of difference in WI also reflected that moisture was uniform in both fields. The RWC ranged from 9 to 13 for field 9 and from 10 to 15 for field 10. Even in these fields there was some heterogeneity in the spatial distribution of f_R as observed by the standard error, as would be expected from in-field spatial variability, but this heterogeneity was < 2% of the mean.

3.2. Moisture correction

Reflectance of the SWIR bands used for NDTI (Fig. 3) and SINDRI (Fig. 4) decreased linearly with WI for each field. Although slight differences in the slope were observed for each band and field, overall the tendency was similar. When the wetness index increased, the numerator of both residue indices remained nearly constant while the denominator decreased. Thus, both NDTI and SINDRI increased as water content increased.

The *slope* to correct the reflectance for NDTI by WI that provided the minimum $RMSE_{Non}$ was 0.971; whereas the *slope* to correct SINDRI bands was 0.358. The new residue indices calculated using the corrected bands, NDTI* and SINDRI*, showed less variation between the wet and dry wedges within each field (Table 2). No significant differences for mean SINDRI* between wet and dry wedges were observed within any of the fields.

The *RMSE* of the f_R based on NDTI* decreased in all fields when compared with the f_R based on NDTI, the $RMSE_{Non}$ declined from 22.7

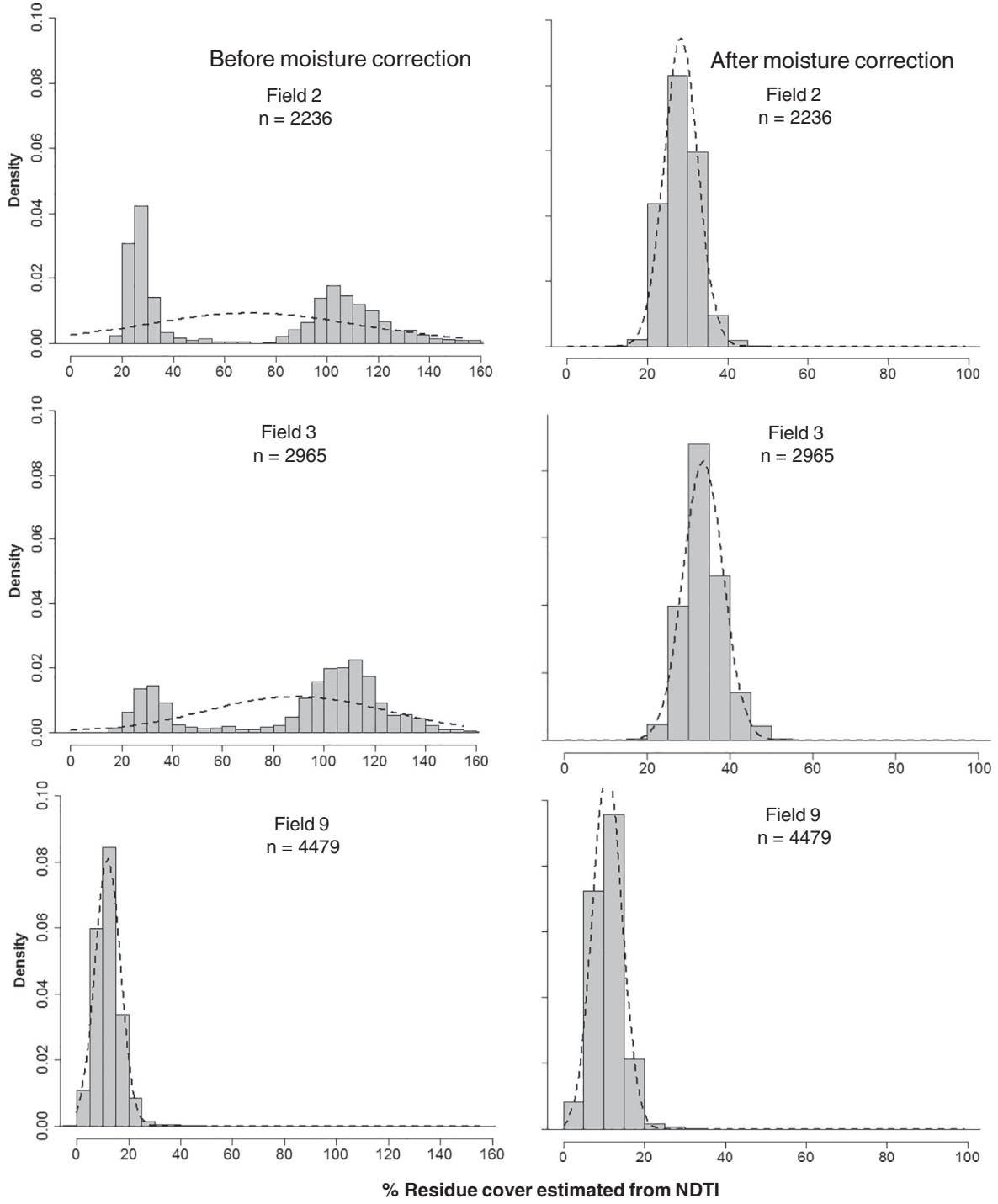

Fig. 5. Probability density function of the percentage of residue cover estimated from NDTI before and after moisture correction for each pixel of the fields 2 and 3 (partially irrigated) and field 9 (uniform moisture distribution). Density is the probability of a pixel to fall within a crop residue cover class (i.e. 10–20%). n is the number of pixels per field.

to 4.7, and the $Range_{max}$ declined from 102 to 19 (Table 3). After moisture correction, the lowest *RMSE* between wedges when estimating f_R from NDTI* was 1.2% (field 4) and the highest 9.2 (field 5). For SINDRI, the moisture correction decreased *RMSE* in most fields, $RMSE_{Non}$ decreased from 6.0 to 2.2, and the $Range_{max}$ from 26 to 10 (Table 3). The highest *RMSE* between wedges when estimating f_R from SINDRI* was 2.8% (field 7), and the lowest 1.1% (field 6). This represented a substantial improvement in accuracy for both moisture corrected indices.

In fields 9 and 10, which had a uniform spatial distribution of RWC, estimation of f_R from residue indices was improved only slightly by moisture correction (Table 3). In field 9 the *RMSE* of f_R decreased from 4.9 if estimated using NDTI to 4.3 from NDTI*, and from 1.7 using SINDRI to 1.1 using SINDRI* (Table 3). Results for field 10 were similar. This result reflected the minimal variability in moisture content within the non-irrigated fields.

3.3. Histograms, and graphical representation

The moisture corrections changed the distributions of WI, NDTI, SINDRI and f_{R_NDTI} and f_{R_SINDRI} in each of the 10 fields. Overall, the results reinforce the previous finding remarked on the wedge analysis.

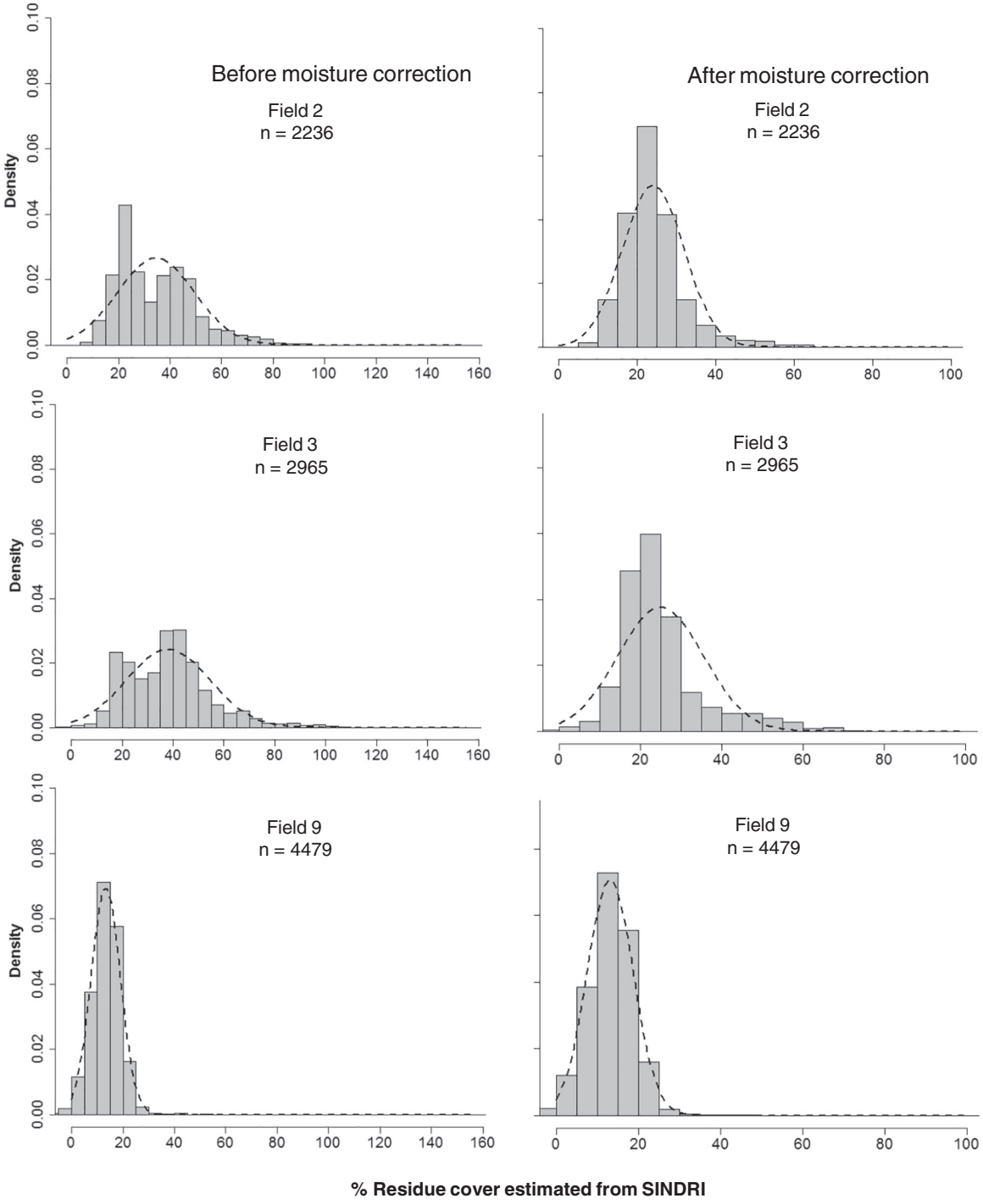

Fig. 6. Probability density function of the percentage of residue cover estimated from SINDRI before and after moisture correction for each pixel of the fields 2 and 3 (partially irrigated) and field 9 (uniform moisture distribution). Density is the probability of a pixel to fall within a crop residue cover class (i.e. 10–20%). *n* is the number of pixels per field.

The variance of the probability density distribution of WI was at least 20 times larger in fields 1 to 8 than in fields 9 and 10, and was particularly large in fields 1, 2 and 3, which had the largest differences in moisture between dry and wet wedges (Table 4). The mean f_R estimated for both residue indices decreased after moisture correction for all fields (Table 4). This decrease was larger for f_{R_NDTI} than for f_{R_SINDRI}, confirming both that SINDRI is more robust than NDTI to moisture conditions, and that the moisture correction proposed in this article significantly reduced the effects of variable moisture conditions on NDTI. For fields 1 to 8, mean f_{R_NDTI} was 68% before moisture correction but 44% after moisture correction. The largest corrections were in fields 2 and 3 in which $f_{R\_NDTI_*}$ was 2.5 times lower than f_{R_NDTI}.

The mean f_R estimated from SINDRI was reduced from 41% to 35% when corrected by moisture (Table 4), with the largest ratio of $f_{R\_SINDRI_*}$ to f_{R_SINDRI} equal to 1.5. The effects of moisture correction on f_R estimated from the residue indices were also evident in the reduction of the variance, a measure of the dispersion, in fields 1 to 8 and to a lesser extent in fields 9 and 10. Even in the fields with relatively uniform moisture distribution, there was spatial variability and room for correction.

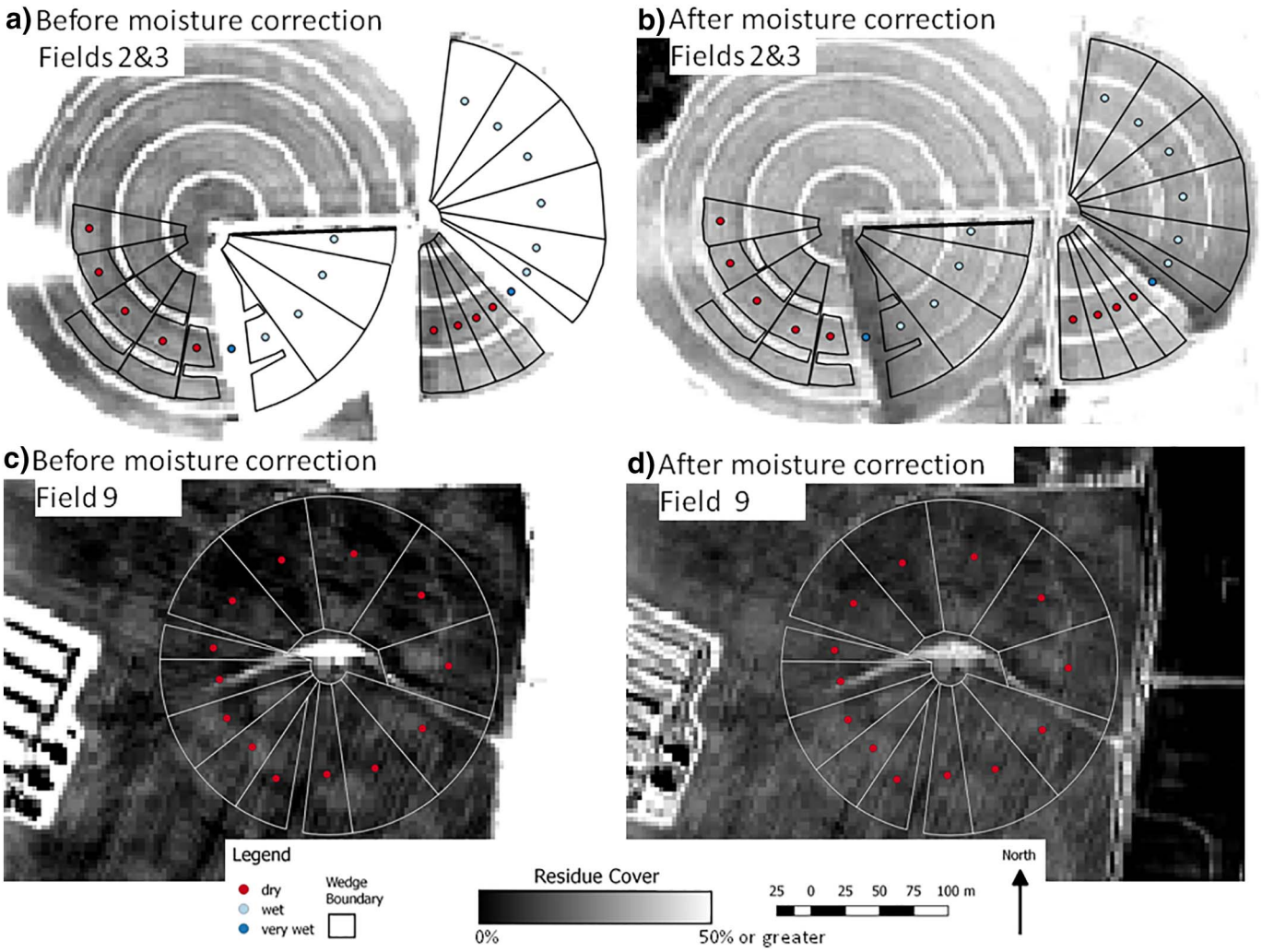

Fig. 7. Image of residue cover estimated from NDTI before and after moisture correction for fields 2 and 3 (partially irrigated) and field 9 (uniform moisture distribution).

To illustrate the effects of moisture correction, we will focus on fields 2, 3 and 9. Moisture corrections are more relevant in fields with high WI variability than in fields with low WI variability. Pixels in fields 2 and 3 that had high RWC were corrected to a larger extent than pixels in field 9 with a uniform moisture distribution (Figs. 5 and 6). The moisture corrections clearly reduced the dispersion of the distribution for fields 2 and 3 whereas the effect for field 9 was minimal. In fields 2 and 3, f_{R_NDTI} showed a bi-modal distribution with pixels distributed in two groups, one around 30% and the other much higher, other around 110–120% (Fig. 5). The moisture correction particularly influenced the second group of pixels, in which wetness induced f_R over-estimation. After correction, $f_{R\_NDTI_*}$ distribution in fields 2 and 3 had a single modal peak centered around 30%. In field 9, with uniform moisture, the probability density distribution of both, f_{R_NDTI} and $f_{R\_NDTI_*}$, had a single maximum peak. When f_R was estimated from SINDRI, the moisture correction diminished the pixels dispersion but all the histograms presented a single peak before and after the moisture correction (Fig. 6), showing that the SINDRI index is more resistant to the effects of moisture. The f_{R_NDTI} and f_{R_SINDRI} images provide visual evidence that pixels in the wet areas f_{R_NDTI} and f_{R_SINDRI} were higher than in the dry areas, and that moisture corrections mitigated the differences (Figs. 7 and 8). For both histograms and images, the differences were larger in f_R estimated from NDTI than from SINDRI, which supports our hypothesis that SINDRI is more robust than NDTI to variations in moisture conditions.

4. Discussion

Water contents of residues and soils often vary spatially across fields with minor changes in topographic relief, and temporally with local meteorological conditions. These variations in water content also significantly affect remotely sensed estimates of f_R (Serbin et al., 2009; Wang et al., 2013). Thus, in order to provide reliable estimates of f_R at local to regional scales, the impact of moisture must be mitigated. However, reliable methods for mitigating the effects of spatially variable water contents on remotely sensed estimates of f_R have not been developed. We have proposed a robust protocol that can be easily implemented for correcting the reflectance of the SWIR bands used by the residue indices, by using a spectral water index that is related to the relative water content of soils and residues. The protocol for correcting f_R was evaluated using wet and dry areas of fields with center pivot irrigation systems that had partially irrigated the fields when the image was acquired.

NDTI is very sensitive to varying moisture conditions (Serbin et al., 2009). Landsat bands, used for NDTI, are relatively wide and interact with several water bands, which means that water content of each pixel is particularly crucial for estimating f_R. Quemada and Daughtry (2016) reported that NDTI accurately assessed f_R under relatively dry conditions (RWC < 0.25), but as moisture conditions increased NDTI significantly overestimated f_R. Other studies successfully used NDTI to distinguish between a few tillage intensity classes, but spatial variations

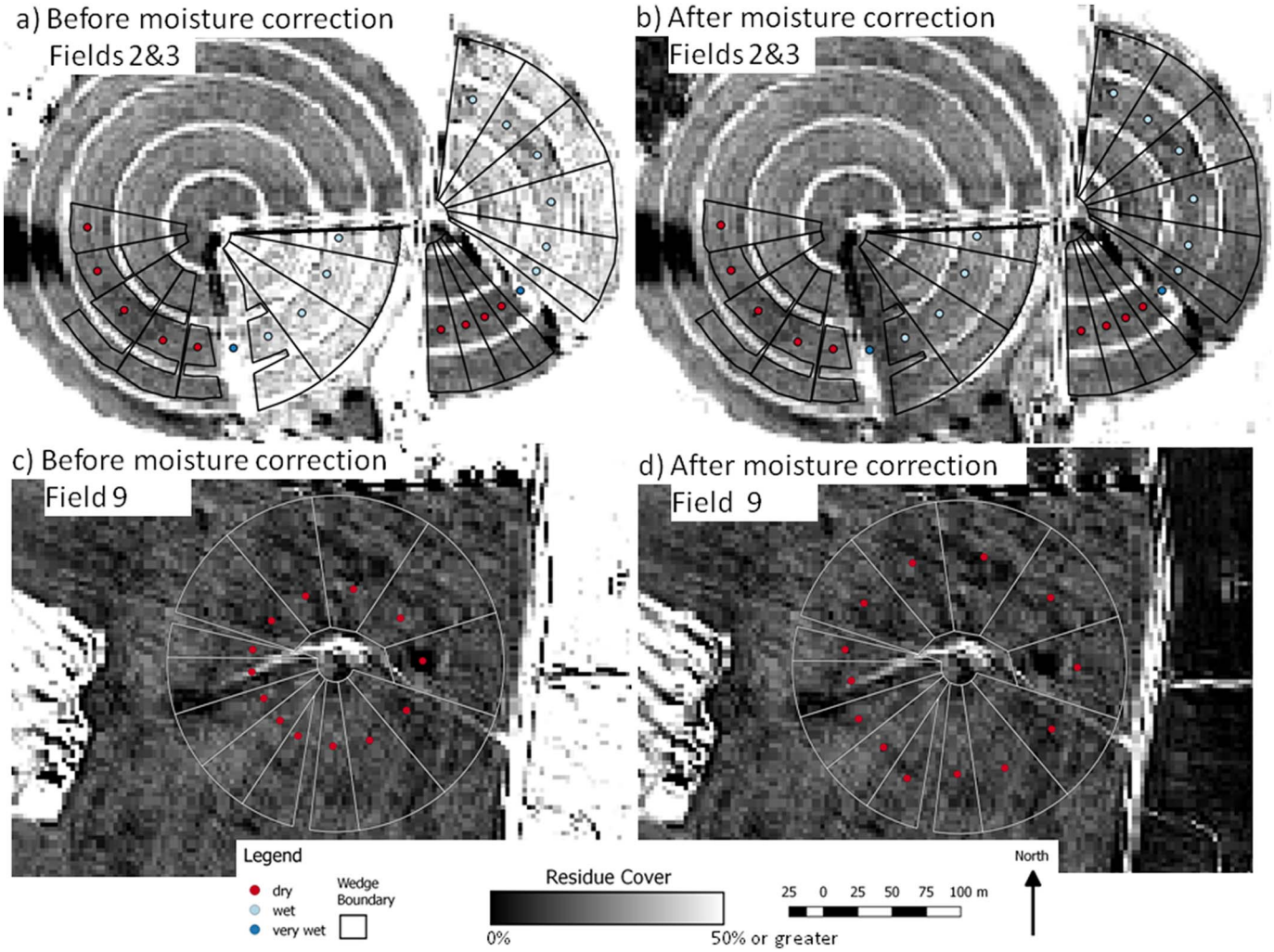

Fig. 8. Image of residue cover estimated from SINDRI before and after moisture correction for fields 2 and 3 (partially irrigated) and field 9 (uniform moisture distribution).

in moisture conditions were probably small because, in each case, the test site was within a single Landsat image (Van Deventer et al., 1997; Sullivan et al., 2008; Galloza et al., 2013). In a multi-temporal study, Gelder et al. (2009) attempted to avoid the problem by selecting only Landsat images that were acquired > 2 days after a precipitation event.

At spatial scales larger than a single field, tillage and planting operations typically occur over a period of several weeks. A single satellite image can provide a snapshot of tillage conditions for a single date, but multiple images are required to track the progress of tillage and planting operations over regional scales. Zheng et al. (2012, 2013) demonstrated that the minimum NDTI values selected from a series of Landsat images acquired during the planting season provided better estimates of tillage intensity than using a single image. With the availability of Landsat (NASA, 2017) and Sentinel-2 (European Space Agency, 2017) images, multi-temporal techniques should benefit greatly from moisture corrections within and among images. Reliable spatially explicit information documenting f_R and tillage intensity would improve the performance of models that predict the impact of agricultural management practices on soil, water, and air quality (Izaurralde et al., 2006; Gassman et al., 2007).

In another study using SWIR satellite imagery, SINDRI was more robust than other spectral indices for estimating f_R even under wet conditions (Serbin et al., 2009). Quemada and Daughtry (2016) proposed using pairs of spectral indices - one for the RWC and another for f_R - to build multivariate models that mitigated the moisture effect; however, calibration parameters required a dataset with abundant ground measurements. In this study, we first used a water index to correct the reflectance of each SWIR band for each pixel of a satellite image, and then used corrected SINDRI* or NDTI* to measure percent fractional residue. Reflectance in each SWIR band decreased linearly and followed similar slopes as the WI increased; therefore, the correction can be conducted with a single factor.

The regression slopes were not the same in all fields (Figs. 3 & 4). The reason for the different regression slopes is not clear. It was not related to crop residue type or f_R level. The water content of soil and crop residues is not homogenous and is affected by soil texture and litter decomposition (Quemada and Cabrera, 2002; Quemada, 2005). Stage of organic residues decomposition varies with time (Quemada and Menacho, 2001) and affects SWIR residue indices (Delgado, 2010). Although optimizing the regression slope in each field separately provided a somewhat lower overall *RMSE* (data not shown), optimizing the regression slope for all the fields together is more appropriate for large-scale applications. Additional information about the local soil types, moisture conditions, and type of crop residues may improve estimates of the changes in reflectance of the SWIR bands relative to water content.

Clearly, reliable remotely sensed estimates of f_R must account for temporal and spatial variation in water content of soils and crop residues. The purpose of this study was not to examine the ability of different spectral indices to assess moisture conditions, but to emphasize the advantages of coupling water and residue indices to mitigate the moisture effect. Spectral indices using various combinations of near-infrared and SWIR bands have been correlated with the water content of leaves (Hunt and Rock, 1989; Hunt Jr et al., 2016), plant canopies

(Hardisky et al., 1983; Gao et al., 2015) and soils (Lobell and Asner, 2002; Whiting et al., 2004). We used the WI based on the ratio between SWIR3 and SWIR5 WV-3 bands because it was proposed as a good indicator of soil and crop residue RWC (Quemada and Daughtry, 2016). The ratio between OLI6 and OLI7 Landsat OLI bands was also proposed as an indicator of RWC, and in our present dataset both water indices, SWIR3/SWIR5 and OLI6/OLI7, were highly correlated ($r^2 = 0.99$) and could be used interchangeably. Additional information could be used to estimate moisture scene conditions, e.g. direct measurements of soil moisture or microwave measurements, but coupling water and residue indices from the same pixel spectra facilitates the implementation of moisture correction and avoids additional uncertainties linked to geospatial references. The strategy of coupling spectral indices could also be applied to distinguish other confounded effects, such as the identification of yellowing vegetation interspersed in green photosynthetic canopies (Prabhakara et al., 2015).

5. Conclusions

Analysis of partially irrigated fields located within WorldView-3 SWIR satellite imagery provided a unique opportunity to evaluate the effect of moisture on indices associated with measurement of crop residue, under non-vegetated conditions. The Shortwave Infrared Normalized Difference Residue Index (SINDRI) was more robust than the Normalized Difference Tillage Index (NDTI) for estimating crop residue cover under varying moisture conditions, although both were affected by moisture. Correcting the reflectance of each spectral band with a water index substantially mitigated the adverse effects of moisture on residue cover estimation. Using a pair of spectral indices, one for moisture content and one for residue cover, improved the overall accuracy of both SINDRI and NDTI for estimating crop residue cover in satellite images. Clearly, the estimates of residue cover or tillage intensity should be based on SINDRI when WV-3 bands are available. However, for regional scale assessments, only Landsat and Sentinel-2 can provide the wall-to-wall coverage required. Crop residue cover and soil tillage intensity can be reliably estimated using NDTI if the uncertainties caused by variable moisture conditions are mitigated.

Acknowledgement

This research was funded by the U.S. Department of Agriculture, Agricultural Research Service (USDA-ARS), the U.S. Geological Survey (USGS) Land Change Science Program, and the Spanish Ministry of Education through the program Salvador de Madariaga and the Comunidad de Madrid (S2013/ABI2717). We would like to thank the staff from USDA-ARS and the U.S. Forest Service International Visitor Program for their helpful assistance. USDA is an equal opportunity provider and employer. Any use of trade, firm, or product names is for descriptive purposes only and does not imply endorsement by the U.S. Government.

The data used to support the findings presented in this manuscript are available online in Science Base at https://doi.org/10.5066/F7FF3R8Z (Quemada et al., 2017). Supplementary data associated with this article can be found in the online version, at https://doi.org/10.1016/j.rse.2017.12.012.

References

Abrams, M., 2000. The Advanced Spaceborne Thermal Emission and Reflection Radiometer (ASTER): data products for the high spatial resolution imager on NASA's Terra platform. Int. J. Remote Sens. 21 (5), 847–859.

Biard, F., Baret, F., 1997. Crop residue estimation using multiband reflectance. Remote Sens. Environ. 59 (3), 530–536.

Booth, D.T., Cox, S.E., Berryman, R.D., 2006. Point sampling digital imagery with 'SamplePoint'. Environ. Monit. Assess. 123 (1), 97–108.

Corak, S.J., Kaspar, T.C., Meek, D.W., 1993. Evaluating methods for measuring residue cover. J. Soil Water Conserv. 48 (1), 70–74.

CTIC, 2015. Crop Residue Management Survey System. Conservation Technology Information Center, West Lafayette, IN, USA.

Daughtry, C.S.T., 2001. Discriminating crop residues from soil by shortwave infrared reflectance. Agron. J. 93 (1), 125–131.

Daughtry, C.S.T., Hunt, E.R., 2008. Mitigating the effects of soil and residue water contents on remotely sensed estimates of crop residue cover. Remote Sens. Environ. 112 (4), 1647–1657.

Delgado, J.A., 2010. Crop residue is a key for sustaining maximum food production and for conservation of our biosphere. J. Soil Water Conserv. 65 (5), 111A–116A.

European Space Agency, 2017. Available online: http://www.esa.int/Our_Activities/Observing_the_Earth/Copernicus/Sentinel-2 (accessed on 20 September 2017).

FAO, 2015. Food and Agriculture Organization of the United Nations. Available online. http://www.fao.org/ag/ca/1a.html (accessed on 20 September 2017).

Galloza, M.S., Crawford, M.M., Heathman, G.C., 2013. Crop residue modeling and mapping using Landsat, ALI, Hyperion, airborne remote sensing data. IEEE J. Sel. Top. Appl. Earth Obs. Remote Sens. 6 (2), 446–456.

Gao, Y., Walker, J.P., Allahmoradi, M., Monerris, A., Ryu, D., Jackson, T.J., 2015. Optical sensing of vegetation water content: a synthesis study. IEEE J. Sel. Top. Appl. Earth Obs. Remote Sens. 8 (4), 1456–1464.

Gassman, P.W., Reyes, M.R., Green, C.H., Arnold, J.G., 2007. The soil and water assessment tool: historical development, applications, and future directions. Trans. Am. Soc. Agric. Biol. Eng. 50 (4), 1211–1250.

Gelder, B.K., Kaleita, A.L., Cruse, R.M., 2009. Estimating mean field residue cover on midwestern soils using satellite imagery. Agron. J. 101 (3), 635–643.

Hardisky, M.A., Klemas, V., Smart, R.M., 1983. The influence of soil-salinity, growth form, and leaf moisture on the spectral radiance of *Spartina alterniflora* canopies. Photogramm. Eng. Remote. Sens. 49, 77–83.

Hobbs, P.R., Sayre, K., Gupta, R., 2008. The role of conservation agriculture in sustainable agriculture. Philos. Trans. R. Soc. B 363 (1491), 543–555.

Hunt Jr., E.R., Daughtry, C.S.T., Li, L., 2016. Feasibility of estimating leaf water content using spectral indices from WolrdView-3's near-infrared and shortwave infrared bands. Int. J. Remote Sens. 37 (2), 388–402.

Hunt, E.R., Rock, B.N., 1989. Detection of changes in leaf water content using near- and middle-infrared reflectances. Remote Sens. Environ. 30 (1), 43–54.

Izaurralde, R.C., Williams, J.R., McGill, W.B., Rosenberg, N.J., Jakas, M.Q., 2006. Simulating soil C dynamics with EPIC: model description and testing against long-term data. Ecol. Model. 192 (3), 362–384.

Kokaly, R.F., Clark, R.N., 1999. Spectroscopic determination of leaf biochemistry using band-depth analysis of absorption features and stepwise multiple linear regression. Remote Sens. Environ. 67 (3), 267–287.

Lobell, D.B., Asner, G.P., 2002. Moisture effects on soil reflectance. Soil Sci. Soc. Am. J. 66 (3), 722–727.

NASA, 2017. International Space Station. Available online. http://www.nasa.gov/mission_pages/landsat/main (accessed on 20 September 2017).

Prabhakara, K., Hively, W.D., McCarty, G.W., 2015. Evaluating the relationship between biomass, percent groundcover and remote sensing indices across six winter cover crop fields in Maryland, United States. Int. J. Appl. Earth Obs. Geoinf. 39, 88–102.

Quemada, M., 2005. Predicting crop residue decomposition using moisture adjusted time scales. Nutr. Cycl. Agroecosyst. 70 (3), 283–291.

Quemada, M., Cabrera, M.L., 2002. Characteristic moisture curves and maximum water content of two crop residues. Plant Soil 238 (2), 295–299.

Quemada, M., Daughtry, C.S.T., 2016. Spectral indices to improve crop residue cover estimation under varying moisture conditions. Remote Sens. 8 (8), 660.

Quemada, M., Menacho, E., 2001. Soil respiration 1 year after sewage sludge application. Biol. Fertil. Soils 33, 344–346.

Quemada, M., Hively, W.D., Daughtry, C.S.T., Lamb, B.T., Shermeyer, J., 2017. Datasets Related to Crop Residue, Irrigation, and Shortwave Infra-red (SWIR) Spectral Reflectance, Talbot County, MD, May 2015: U.S. Geological Survey Data Release. http://dx.doi.org/10.5066/F7FF3R8Z.

Serbin, G., Hunt, E.R., Daughtry, C.S.T., McCarty, G.W., Doraiswamy, P.C., 2009. An improved ASTER index for remote sensing of crop residue. Remote Sens. 1 (4), 971–991.

SIC, 2017. Satellite Imaging Corporation. Available online. http://www.satimagingcorp.com/satellite-sensors/worldview-3/ (accessed on 20 September 2017).

Sullivan, D.G., Strickland, T.C., Masters, M.H., 2008. Satellite mapping of conservation tillage adoption in the Little River experimental watershed, Georgia. J. Soil Water Conserv. 63 (3), 112–119.

Thoma, D.P., Gupta, S.C., Bauer, M.E., 2004. Evaluation of optical remote sensing models for crop residue cover assessment. J. Soil Water Conserv. 59 (5), 224–233.

Van Deventer, A.P., Ward, A.D., Gowda, P.H., Lyon, J.G., 1997. Using thematic mapper data to identify contrasting soil plains and tillage practices. Photogramm. Eng. Remote. Sens. 63, 87–93.

Wang, C.K., Pan, X.Z., Liu, Y., Li, Y.L., Shi, R.J., Zhou, R., Xie, X.L., 2013. Alleviating moisture effects on remote sensing estimation of crop residue cover. Agron. J. 105 (4), 967–976.

Whiting, M.L., Li, L., Ustin, S.L., 2004. Predicting water content using Gaussian model on soil spectra. Remote Sens. Environ. 89 (4), 535–552.

Zheng, B., Campbell, J.B., de Beurs, K.M., 2012. Remote sensing of crop residue cover using multi-temporal Landsat imagery. Remote Sens. Environ. 117, 177–183.

Zheng, B., Campbell, J.B., Serbin, G., Daughtry, C.S.T., 2013. Multi-temporal remote sensing of crop residue cover and tillage practices: a validation of the minNDTI strategy in the United States. J. Soil Water Conserv. 68 (2), 120–131.

Zheng, B., Campbell, J.B., Serbin, G., Galbraith, J.M., 2014. Remote sensing of crop residue and tillage practices: present capabilities and future prospects. Soil Tillage Res. 138, 26–34.